ChemPubSoc Europe
DOI: 10.1002/cptc.201900063
CHEMPHOTOCHEM Articles

A Semisynthetic Peptide–Metalloporphyrin Responsive Matrix for Artificial Photosynthesis

Zhongwu Sun,*[a] Christoph A. Diebolder,[b] Ludovic Renault,[b] and Huub de Groot*[a]

The CsmA protein from the baseplate of the *Chlorobaculum tepidum* is proposed as an attractive motif for the engineering of semisynthetic materials for artificial photosynthesis. We perform self-assembly of zinc protoporphyrin IX (ZnPP) with a truncated CsmA (tCsmA) amphipathic peptide scaffold for the bottom-up construction of a semisynthetic matrix for energy transfer. The resulting self-assembly shows an extended periodic structure with 7_2 helical symmetry. The complex is able to maintain a good photostability for at least 30 min when the concentration is more than 20 μM, and almost 100% harvested energy can be transferred to the acceptor cation radical methyl viologen (MV^+). The excitation-energy transfer rate of the complex was increased from the ns^{-1} scale to the ps^{-1} scale that is comparable to natural light-harvesting antenna systems. It contributes to converging evidence that chiral responsive matrix assemblies can be developed for efficient light energy harvesting in artificial photosynthesis.

1. Introduction

Solar energy is a major source of renewable energy with the potential to address major sustainability challenges the world is facing. A finite supply of low carbon electricity from photovoltaics and wind can be followed by electrolysis to produce fuels, but such adiabatic conversion and concentration chains are not optimally efficient. In contrast, nature makes abundant use of non-adiabatic conversions that transiently violate detailed balance for high yield.[1] Photosynthesis uses ordered arrays of pigments for energy or charge transfer.[2] Traditionally, transmission of exciton energy is thought to proceed via the Förster or Dexter exciton transfer mechanisms.[3] However, photosynthetic proteins are chiral assemblies which undergo light-driven conformational changes and self-select vibrations to develop vibronic states for driving semi-classical coherent transfer with nearly 100% yield in lossless processes, a concept known as the responsive matrix.[4]

The critical step in constructing a responsive matrix is the chemical engineering of a chiral module. Here we start from a zinc protoporphyrin IX (ZnPP) chromophore and provide a new paradigm for energy transfer in a semisynthetic matrix for artificial photosynthesis.[5] We use a truncated CsmA (tCsmA) construct, containing 43 amino acids, which is derived from the helical CsmA peptide from the baseplate of *Chlorobaculum tepidum*. This is the smallest light-harvesting protein known in nature, and coordinates a single BChl *a* (Figure S1 in the Supporting Information). The tCsmA was modified by removing the flexible segments from the N and C-terminal, which attach to the lipid monolayer confining the chromosome and the FMO complex respectively, leaving the functional central α-helix (Figure 1 and Supporting Information S1). In nature, dimers of CsmA-BChl *a* self-assemble to form extended para-crystalline layers with BChl *a* in CsmA strands.[6] The system assists in energy transfer and storage from the chlorosome to the FMO antenna and the photosynthetic reaction center in *Chlorobaculum tepidum*.[7] NMR studies of monomeric CsmA in solution have shown that it is a α-helical amphipathic peptide.[8] With the exception of the single coordinating histidine in the sequence, all potentially charged residues, like lysine and arginine, are located on one side of the helix (Figure 1).

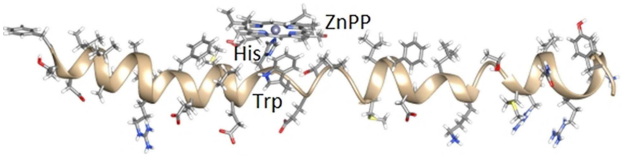

Figure 1. Putative model structure of the tCsmA in complex with ZnPP derived from the CsmA-BChl *a* complex.

With the assistance of tCsmA scaffolds, ZnPP is bound to form a molecular wire with complexation via slow dialysis.[9] We perform initial assays of the light harvesting, indicating that excitons formed in the array upon photoexcitation have lifetimes on the ns scale, comparable to ZnPP in solution.[10] When a quencher methyl viologen (MV) is used in excess to accept the harvested light energy from ZnPP, nearly 100% of the fluorescence is rapidly quenched, consistent with a high

[a] Z. Sun, Dr. H. de Groot
Leiden University
Leiden Institute of Chemistry
2333 AL Leiden (The Netherlands)
E-mail: z.sun@lic.leidenuniv.nl
groot_h@lic.leidenuniv.nl
[b] Dr. C. A. Diebolder, Dr. L. Renault
Leiden University
The Netherlands Centre for Electron Nanoscopy (NeCEN)
2333 AL Leiden (The Netherlands)

Supporting information for this article is available on the WWW under https://doi.org/10.1002/cptc.201900063

efficiency of excitation-energy transfer from the ZnPP wires to the MV.[11]

2. Results and Discussion

2.1. Constitution and Characterization

An important finding of our studies is that slow dialysis is key to form a tCsmA-ZnPP complex, since the complex is moderately soluble while the components precipitate upon dialysis. The 1-propanol, which is thought to cover the hydrophobic side of randomly aggregated tCsmA, is slowly removed by dialysis against KPi buffer. This exposes the histidine, which is the only charged residue at the hydrophobic side and is the binding site for coordination to ZnPP. UV/Vis absorption spectroscopy indicates histidyl axial binding of the chromophore by characteristic bathochromic shifts around 15 nm relative to the monomeric ZnPP in solution (Figure 2A).[5b,12] As a control experiment, we performed dialysis of either the ZnPP or the tCsmA in 50 mM KPi buffer containing 6 M 1-propanol and it was found that both precipitate upon dialysis against KPi buffer (blue trace in Figure 2A). This suggests that dialysis should be slow compared to the binding to prevent precipitation of separate components. The B-band shifts by 14 nm, from 416 nm to 430 nm, while the Q(1,0) and Q(0,0) bands shift by 8 and 7 nm to 554 nm and 590 nm, respectively, after constitution (Figure 2A). These shifts are well in line with literature data collected from semi-artificial systems, which consistently show shifts in the range of 10–15 nm for the B-band.[5a, 13] After binding, the absorption in the Q(1,0) band of the tCsmA-ZnPP complex is stronger than for the Q(0,0) band, while for the ZnPP monomer the absorption for the Q(1,0) band is less than for the Q(0,0) band. The relative intensities of these bands correlate with the stability of the complex, and the decrease of the Q(0,0) band relative to the Q(1,0) band upon formation of the complex indicates that binding enhances the stability of the complex with a square-planar Zn^{2+} in the porphyrin.[14] Moreover, the CD spectrum in Figure S4 for the secondary structure reveals the maintenance of a helical structure only when the ZnPP is bound. Therefore the slow dialysis is vitally important for the self-assembly of an intact helix structure with tCsmA bound to ZnPP.

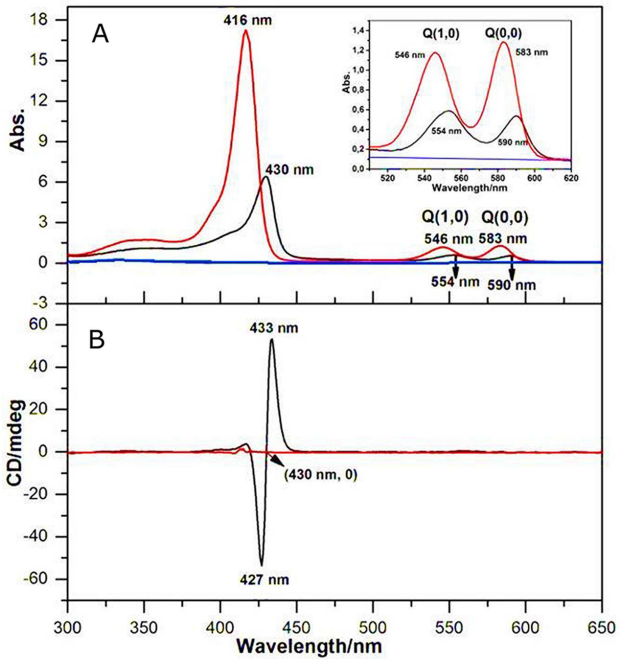

Figure 2. (A) UV/Vis absorption and (B) corresponding CD spectra, collected from 50 μM tCsmA-ZnPP complex in 50 mM KPi buffer (black) and 50 μM ZnPP in 50 mM KPi buffer containing 6 M 1-propanol (red). The blue line shown in panel A is the residual UV response from KPi buffer after dialysis, *i.e.* without tCsmA, confirming that ZnPP has precipitated. The Q band region is shown in panel A. The concentration of peptide at the start of the dialysis is 50 mM in KPi buffer with 6 M 1-propanol and there is no CD response (B, red trace). Upon complex formation a CD response is detected (B, black trace).

At pH = 7.9 and with five times molar excess of ZnPP relative to the concentration of peptide, the binding optimally proceeds, with an efficiency of ~ 60–70% over a peptide concentration range of 40–130 μM (Figure S2). UV/Vis absorption spectra showed a narrow singlet peak at 430 nm, which indicates high purity. The concentration of protein has little influence on the binding efficiency. Similar to the natural CsmA-BChl *a* complex, the tCsmA-ZnPP complex shows oligomer bands on the SDS gel (Figure S3).[15] The complex is stable during three months storage in the dark at 4 °C. The molar extinction coefficient of the ZnPP in complex with tCsmA is 117400 $M^{-1}cm^{-1}$ and was determined by the combined use of UV-Vis and ICP-OES (Figure S5 and Table S1).[16] With a subsequent BCA assay, a stoichiometry of tCsmA:ZnPP ~ 1:1 was determined (Supporting Information S3).

Under cryo-conditions of Transmission Electron Microscopy (TEM) the images show long filaments (Figure 3A). We performed maximum likelihood 2D classification of 99142 particles using a mask size of 535 Å, corresponding with a box size of 610 pixels. All 50 2D class averages show the same chain-like structure (Figure S6).[17] The diameter of a filament is about 5 nm (Figure 3B). As the Fast Fourier Transform (FFT) Figure 3C shows, multiple layer lines separated by 1/22.6 nm^{-1} provide converging and convincing evidence for a helical structure with a C = 22.6 ± 0.02 nm periodic repeat. The strongest peaks close to the meridian are on the second layer line, corresponding with a helix pitch p = 11.3 ± 0.02 nm, i.e. half of the repeat (Figure 3C). The seventh layer line with intensity on the meridian reveals a helical rise h = 3.23 ± 0.02 nm, and according to the FFT the complex forms a 7_2 helix. A proposed assembly is shown in Figure 3D. The high density parts inside the filaments can be attributed to tetrameric units of tightly packed ZnPP (Figure 3B, labelled with the red circle). The size of the ZnPP clusters is ~1.2 nm, and they are separated by ~2 nm. In addition, most likely the system self-assembles as a symmetric double helix.

Linear Dichroism (LD) allows to determine the macroscopic orientation from the absorption of parallel and perpendicular linearly polarized light, and to study the orientation of the ZnPP in the filaments, we collected LD data along with

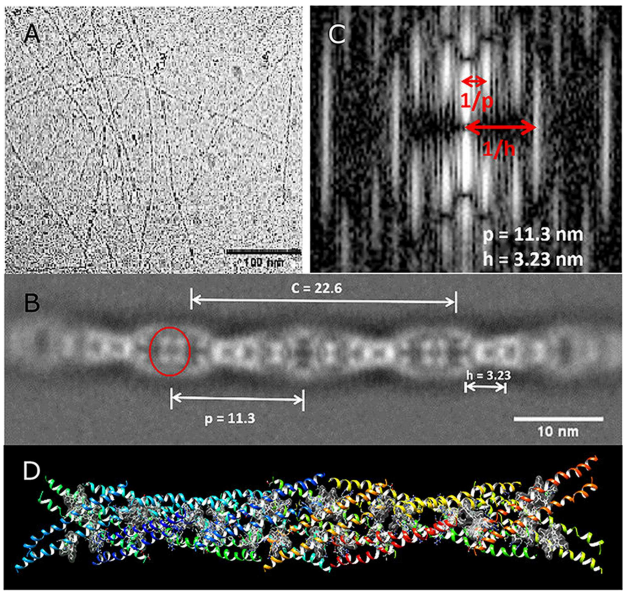

Figure 3. (A) cryo-EM image showing individual filaments in a sample of 200 μM tCsmA-ZnPP complex in KPi buffer. (B) 2D class average of particles from cryo-EM images. (C) Fast Fourier Transform of a 2D class average (Figure 3B). (D) Proposed assembly model according to the parameters from the 2D class average. Each subunit has a different colour and the ZnPP are depicted in light grey. Due to the image processing, there is a contrast inversion from A to B.

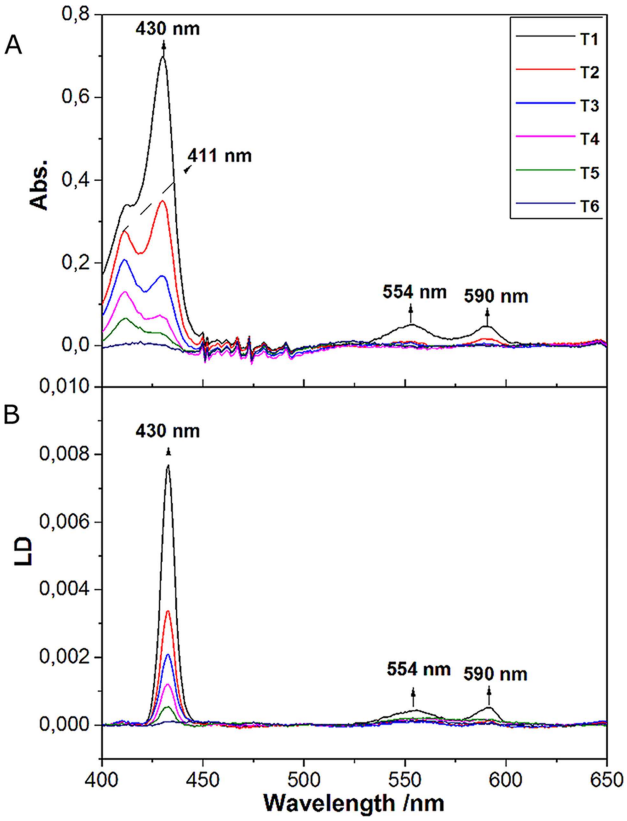

Figure 4. (A) UV/Vis absorption and (B) corresponding LD spectra. The spectrum T1 corresponds to the first measurement, T2 was collected after 7 min, T3 after 13 min, T4 after 19 min, T5 after 30 min and T6 after 1 h 14 min.

simultaneous UV-Vis absorbance spectra in a squeezing gel. According to the UV-Vis results (Figure 4A), an additional 411 nm ZnPP peak appears, in contrast with the UV-Vis data collected from the complex in solution (black trace in Figure 2A). The shift to 411 nm is attributed to loss of binding and decomposition by squeezing gel components (Table S3, Figure S7). The LD spectra measured over time show positive peaks at 430 nm with the two Q band signals at 554 nm and 590 nm, due to vertically oriented ZnPP-tCsmA filaments, along the squeezing direction of the gel (Figure 4B), which indicates a predominantly parallel orientation of ZnPP planes to tCsmA scaffolds as well.[18] This is in line with the results of the 2D class average of filaments (Figure 3B). The lack of orientation for the 411 nm component is consistent with dissociation of the complex, which leads to a randomly oriented ZnPP fraction. The LD confirms that the binding of ZnPP to the tCsmA is necessary to build the supramolecular photosynthetic system.

Compared to the CD response of the monomeric ZnPP in propanol buffer, the B band of the complex at 430 nm shows a high intensity and nearly symmetric Cotton effect (Figure 2B). The strong CD signal observed is from ZnPP motifs interacting with each other and forming a chiral exciton coupled unit, with dipole-dipole interactions between monomers, which is well in line with Figure 3B, where the ZnPP appears to form tetrameric repeat units. In contrast, while the optical response for the ZnPP in propanol buffer in Figure 2A is stronger than for the complex, the CD is virtually absent, which confirms that the ZnPP in solution is monomeric. On the other hand, the CD response for the Q bands is very weak in the CD data collected from the complex. Since the LD data in Figure 4 are in line with a specific orientation angle of the ZnPP relative to the tCsmA scaffolds, and the particle shows a helical structure, the vanished dipole-dipole interaction of the Q bands indicates that the ZnPP possibly form oligomers with exciton coupling at a specific rotation angle in the molecular system to offset the dipole-dipole interaction of the Q bands.[19] Based on LD and TEM data, the ZnPP-CsmA complex probably forms a helical structure that is composed of twisted peptide assemblies built from well-ordered chiral oligomeric units that give rise to a single CD response (Figure 2B).[6,19c,20]

2.2. Photostability

The tCsmA-ZnPP complex forms large soluble particles that show a single distribution peak around 1.07 mL in the SEC data, with the retention indicating a large molecular weight (Figure S8). This is consistent with the formation of extended filaments shown in the TEM data in Figure 3A. In addition, SEC also shows that the complex is quite sensitive to light. The peak shifts to ~1.09 mL after 30 minutes of light exposure, which indicates that the particle size became smaller upon exposure to light. Moreover, steady state fluorescence measurements, which show a slow exponential decay, indicate slow photodissociation or photodegradation of the complex upon

illumination (Figure S9). In the literature it has been reported that the histidyl axial binding of the ZnPP can be unstable under light exposure.[12a] While free ZnPP precipitates in buffer, in the gel the ZnPP can be dissolved and in the LD data in Figure 4A a pronounced free ZnPP signal observed at 411 nm wavelength, indicative of partial dissociation in the gel. Both the 430 nm and the 411 nm response decrease upon illumination, indicating photodegradation for prolonged exposure, but the relative intensity changes in favor of the free ZnPP. With more than 2 h exposure with sunlight or 430 nm UV light, the complex was totally dissociated. The reason for the photodissociation might be that the dissipation of heat is slow.[5b]

As Figure S10 shows, the stability is related to the concentration. At a concentration of about 20 μM the complex is stable for at least 30 minutes (Figure S10A). It has recently been proposed that light-driven conformational changes in chiral protein scaffolds can develop vibronic states within or between linear arrays. In such systems, excitons spread rapidly over the system, which may help to decrease the risk of damage and dissociation rate. However, during long time exposure the light still damages the complex which results in size decrease of the filament. Apparently a high concentration improves the stability, which suggests that distribution of energy helps to dissipate the excess energy and may be of vital importance for further improvement of the stability.

2.3. Exciton-Energy Transfer

To address further the energy transfer potential of the tCsmA-ZnPP self-assembly, an acceptor MV was added.[11d,e,12a,21] Generally, MV exists in the dicationic form MV^{2+} in aqueous solution. However, MV has highly reversible redox reactions, at the reversible potential of E0 = −0.4 ~ −0.55 V and −0.75 ~ −0.9 V vs NHE in aqueous solution.[11c,22] A solution of MV with sodium dithionite contains a mixture of MV^{+} and MV^{2+} (Figure S11). When MV^{2+} is added to a suspension of tCsmA-ZnPP filaments in KPi buffer, fluorescence quenching is hardly observed (Figure S12). This changes when the acceptor is converted to the cation radical form MV^{+} with excess sodium dithionite (Figure S13).[23] As the data show, the tCsmA-ZnPP complex contains 594 nm and 650 nm emission peaks after excitation (Figure S12). On the other hand, the MV^{+} shows a strong broad absorption at 606 nm ($\varepsilon = 13700\ M^{-1}cm^{-1}$), which overlaps with the tCsmA-ZnPP emission (Figure S12).[11d] This leads us to conclude that intermolecular FRET or Dexter energy transfer between ZnPP and MV^{+} may cause fluorescence quenching by energy transfer. The quenching is dependent on the concentration of MV^{+}. When the concentration was increased to about 300 μM MV^{+} in the tCsmA-ZnPP solution, nearly all fluorescence of ZnPP was quenched (Figure 5).

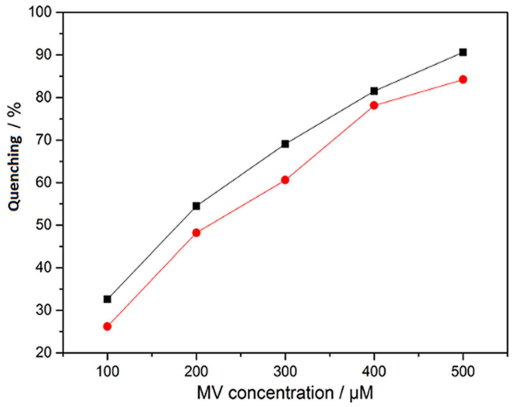

Figure 5. The fluorescence quenching diagram for 3.5 μM tCsmA-ZnPP complex at 594 nm (black trace) and 650 nm (red trace) with different concentration of MV. The solution contains 1.25 mM sodium dithionite. The excitation wavelength is 440 nm.

As Table 1 shows, the exposure to the MV^{+} acceptor reveals excellent energy transfer efficiency from the complex to the MV^{+}. The fluorescence decay responses at 594 nm and 650 nm can be described with 3 different lifetime components. All three lifetimes of the complex with the MV^{+} additive are shortened, especially $\tau 3$ was dramatically shortened to ~1 ps and the energy is almost 100% quenched by the acceptor. Although the time-resolved fluorescence spectroscopy has a limited resolution of 25 ps, $\tau 3$ is about a few picoseconds or even shorter, at the femtosecond time scale. When sodium dithionite was depleted by letting it react with oxygen, the MV^{+} was converted to MV^{2+} and there is no fluorescence quenching. The quenched complex recovered the same fluorescence as without acceptor, indicating that it maintains its integrity upon photoexcitation (Figure S14). This highlights the importance of the MV^{+} as the quenching species.

3. Conclusions

In conclusion, we have employed the dialysis method to gain control over metalloporphyrin forming an organized array with truncated CsmA peptides to develop helical scaffolds. The tCsmA-ZnPP complex forms soluble and stable long-aspect-

Table 1. Fitted time constants of fluorescence transients in tCsmA-ZnPP complex solution with different additives under a 440 nm excitation beam.

Additives	594 nm Lifetime [ns]				650 nm Lifetime [ns]			
Lifetime	τ_1	τ_2	τ_3	$\tau_{average}$	τ_1	τ_2	τ_3	$\tau_{average}$
No MV and $Na_2S_2O_4$	1.63 (9%)	0.5 (32%)	0.11 (59%)	0.37	3.13 (5%)	0.83 (29%)	0.14 (66%)	0.49
MV^{2+} (no $Na_2S_2O_4$)	1.62 (8%)	0.63 (44%)	0.15 (48%)	0.48	2.82 (5%)	0.88 (44%)	0.21 (51%)	0.64
MV^{+} (excess $Na_2S_2O_4$)	1.1 (0.03%)	0.28 (0.12%)	< 0.010 (99.85%)	0.0017	1.3 (0.01%)	0.4 (0.03%)	< 0.010 (99.96%)	0.0017

ratio filaments to encapsulate strongly interacting oligomeric metalloporphyrins for photoexcitation. The solubility of the complex is good compared to the tCsmA starting material, which suggests that the amphipathic tCsmA has its hydrophobic residues on the inside and the hydrophilic residues on the outside. The tCsmA-ZnPP complex obtained by dialysis is well defined, and shows high purity. The single histidine available for binding with metalloporphyrin allows the material to get a stable 1:1 chromophore/peptide binding ratio. The self-assembly of the tCsmA-ZnPP complex shows certain photostability. The photoinduced energy of ZnPP-tCsmA complex can be transferred within few picoseconds with a nearly 100% quenching to MV^+. This artificial antenna system paves the way for the design of semisynthetic building blocks for light energy harvesting in artificial photosynthesis.

Experimental Section

Materials

Zn(II) Protoporphyrin IX (ZnPP) was purchased from Frontier Scientific. The tCsmA, with N-Terminal Acetylation and C-Terminal Amidation, was purchased from GL Biochem Ltd (98% purity). Dimethyl sulfoxide (DMSO, Sigma Aldrich), monobasic dihydrogen phosphate (Sigma Aldrich), dibasic monohydrogen phosphate (Sigma Aldrich), 1-propanol (Sigma Aldrich) and the microdialysis vial (Pierce™ 96-well Microdialysis Plate, 3.5K MWCO, Thermo Fisher Scientific) were used for constitution of tCsmA-ZnPP complexes. MV and sodium dithionite (85% purity) were obtained from Sigma-Aldrich.

Equipment

The concentration of protein was measured with a Microvolume DS-11 Spectrophotometer (DeNovix). The steady state Fluorescence spectra were measured using a FLS900 Fluorescence Spectrometer (Edinburgh Instruments) and Aqualog® Water Treatment Plant Analyzer (HORIBA Scientific). The UV-Vis spectra were measured using a UV-1700 Spectrophotometer (Shimadzu). The molar extinction coefficient of the complex was determined by Vista MPX Simultaneous Inductive Coupled Plasma-Optical Emission Spectrometry (ICP-OES, Varian Inc.). The complex was loaded with a 10 μL injection loop on a SuperdexTM 200 Increase 5/150 GL column (GE Healthcare) to perform Size-Exclusion Chromatography (SEC). Negative stain images were obtained with a JEM-1010 transmission electron microscope with a maximum output voltage up to 70 KV equipped with an Olympus Megaview camera (JEOL Ltd.). The circular Dichroism (CD) spectra were measured using a J-815 CD spectrometer (JASCO). The Linear Dichroism (LD) spectra were measured using a Chirascan CD Spectrophotometer (Applied Photophysics). The time-resolved fluorescence measurements were performed by FluoTime 300 (PicoQuant).

Methods

Constitution of the tCsmA-ZnPP complex was carried out in a 5:1 mixture of ZnPP and tCsmA dissolved in pH 7.9 50 mM Potassium Phosphate buffer (KPi buffer) containing 6M 1-propanol. The ZnPP was added from a 200 mM DMSO solution. The reaction proceeded in the microdialysis vial against 4 times 1.4 mL KPi dialysis buffer at 4 °C in the dark. The dialysis times were 2 hours except for the third one, where the sample was incubated overnight. After the last dialysis step, the sample volume was increased from 100 μL to 130 μL and the sample was centrifuged for 15 minutes at 4 °C with 30,000×*g* to remove unbound CsmA and ZnPP precipitate.

To determine the extinction coefficient, different concentrations of tCsmA-ZnPP complex solutions were prepared. For each aliquot the absorption at 430 nm was measured and the Zn concentration was determined by ICP-OES to calculate the extinction coefficient of the complex. By combining a Bicinchoninic Acid (BCA) assay with the molar extinction coefficient of complex, the stoichiometry was determined.

For Cryo-EM, grids were prepared by placing 4 μL of 200 μM tCsmA-ZnPP complex onto 200 mesh grids with 2 μm holes (Quantifoil R2/2, Quantifoil Micro Tools, GmbH). Grids were glow discharged for 20 seconds prior to plunge freezing in liquid ethane cooled by liquid nitrogen, using a FEI Vitrobot IV at 100% relative humidity, chamber temperature of 4 °C. Data were collected at 300 kV with a Titan Krios electron microscope, using an electron dose of 51 $e^-/Å^2$ and a magnification of 75,000×. The final object sampling was therefore 0.88 Å/pixel. Exposures were recorded using the EPU automated acquisition software on a FEI Falcon II direct electron detector. The single particle analysis was performed with Relion 2.0, while Fiji was used for Fourier transforms of 2D class images.

For LD experiments, a squeezing gel of 5% acrylamide with 50% glycerol was used. To avoid fast degradation of the sample by components of the squeezing gel, the procedure was optimized. All materials were cooled on ice before use. To prepare the gel, all components except the sample were mixed, and put at room temperature for 2.5 minutes. The complex was added and the solution was transferred to the gel squeezer. The system was kept on ice for 5 minutes and another 5 minutes at room temperature and immediately the LD was measured.

For the time-resolved fluorescence measurements, the samples were prepared with 500 μM MV, 1.25 mM sodium dithionite and tCsmA-ZnPP complex in KPi buffer. The excitation beam was 440 nm.

For steady state fluorescence measurements, the samples were prepared with 1.25 mM sodium dithionite and tCsmA-ZnPP complex in KPi buffer with different concentrations of MV. The excitation wavelength was 430 nm for the tCsmA-ZnPP complex. In addition, steady state fluorescence was measured for both samples with 440 nm excitation light, corresponding with the wavelength used in time-resolved fluorescence experiments.

Acknowledgements

The research leading to this work has gratefully received funding from the Chinese Scholarship Council. The authors thank the support of Lijin Tian and Anjali Pandit (SSNMR, Leiden University) for the fluorescence experiments and discussion. The authors also acknowledge Sandrine D'Haene from the department of Biophysics Photosynthesis/Energy, Vrije Universiteit Amsterdam for the LD experiment, and Jos van Brussel from LIC/Metals in Catal, Biomim & Inorg Mat, Leiden Institute of Chemistry for the test of ICP-OES. The microscopy work was performed in the NECEN cryo-EM facility in Leiden. Laura Opdam is acknowledged for critically reading the manuscript.

Conflict of Interest

The authors declare no conflict of interest.

Keywords: artificial photosynthesis · chirality · exciton energy transfer · self-assembly · semisynthetic matrices

[1] a) A. W. Chin, A. Datta, F. Caruso, S. F. Huelga, M. B. Plenio, *New J. Phys.* **2010**, *12*, 065002; b) A. Chin, J. Prior, R. Rosenbach, F. Caycedo-Soler, S. Huelga, M. B. Plenio, *Nat. Phys.* **2013**, *9*, 113; c) S. F. Huelga, M. B. Plenio, *Contemp. Phys.* **2013**, *54*, 181–207.

[2] a) J. Pšenčík, T. Ikonen, P. Laurinmäki, M. Merckel, S. Butcher, R. Serimaa, R. Tuma, *Biophys. J.* **2004**, *87*, 1165–1172; b) N. Adir, *Photosynth. Res.* **2005**, *85*, 15–32.

[3] a) I. McConnell, G. Li, G. W. Brudvig, *Chem. Biol.* **2010**, *17*, 434–447; b) R. Van Grondelle, *Biochim. Biophys. Acta Rev. Bioenerg.* **1985**, *811*, 147–195; c) R. van Grondelle, J. P. Dekker, T. Gillbro, V. Sundstrom, *Biochim. Biophys. Acta Rev. Bioenerg.* **1994**, *1187*, 1–65.

[4] a) R. Purchase, H. De Groot, *Interface Focus* **2015**, *5*, 20150014; b) R. A. Mathies, *Nat. Chem.* **2015**, *7*, 945; c) X. Yin, P. C. Struik, *J. Exp. Bot.* **2015**, *66*, 6535–6549; d) D. P. Hoffman, R. A. Mathies, *Acc. Chem. Res.* **2016**, *49*, 616–625.

[5] a) H. C. Fry, J. M. Garcia, M. J. Medina, U. M. Ricoy, D. J. Gosztola, M. P. Nikiforov, L. C. Palmer, S. I. Stupp, *J. Am. Chem. Soc.* **2012**, *134*, 14646–14649; b) L. Luo, C.-H. Chang, Y.-C. Chen, T.-K. Wu, E. W.-G. Diau, *J. Phys. Chem. B* **2007**, *111*, 7656–7664; c) M. Chromiński, K. ó Proinsias, E. Martin, D. Gryko, *Eur. J. Org. Chem.* **2013**, *2013*, 1530–1537; d) K. Liu, R. Xing, C. Chen, G. Shen, L. Yan, Q. Zou, G. Ma, H. Möhwald, X. Yan, *Angew. Chem. Int. Ed.* **2015**, *54*, 500–505; e) K. Liu, R. Xing, Y. Li, Q. Zou, H. Möhwald, X. Yan, *Angew. Chem. Int. Ed.* **2016**, *55*, 12503–12507; f) K. Liu, C. Yuan, Q. Zou, Z. Xie, X. Yan, *Angew. Chem.* **2017**, *129*, 7984–7988.

[6] J. T. Nielsen, N. V. Kulminskaya, M. Bjerring, J. M. Linnanto, M. Rätsep, M. Ø. Pedersen, P. H. Lambrev, M. Dorogi, G. Garab, K. Thomsen, *Nat. Commun.* **2016**, *7*, 12454.

[7] a) K. J. Milks, M. Danielsen, S. Persson, O. N. Jensen, R. P. Cox, M. Miller, *Photosynth. Res.* **2005**, *86*, 113–121; b) A. Zobova, A. Taisova, E. Lukashev, N. Fedorova, L. Baratova, Z. Fetisova, *J. Biophys.* **2011**, *2011*.

[8] N. V. Kulminskaya, M. Ø. Pedersen, M. Bjerring, J. Underhaug, M. Miller, N. U. Frigaard, J. T. Nielsen, N. C. Nielsen, *Angew. Chem. Int. Ed.* **2012**, *51*, 6891–6895.

[9] Q. Zhou, T. M. Swager, *J. Am. Chem. Soc.* **1995**, *117*, 12593–12602.

[10] J. J. Leonard, T. Yonetani, J. B. Callis, *Biochemistry* **1974**, *13*, 1460–1464.

[11] a) L. A. Summers, *The bipyridinium herbicides*, Academic Press Inc., **1980**; b) J. S. Bus, J. E. Gibson, *Environ. Health Perspect.* **1984**, *55*, 37–46; c) T. Watanabe, K. Honda, *J. Phys. Chem.* **1982**, *86*, 2617–2619; d) V. Proux-Delrouyre, C. Demaille, W. Leibl, P. Sétif, H. Bottin, C. Bourdillon, *J. Am. Chem. Soc.* **2003**, *125*, 13686–13692; e) T. Komatsu, R.-M. Wang, P. A. Zunszain, S. Curry, E. Tsuchida, *J. Am. Chem. Soc.* **2006**, *128*, 16297–16301.

[12] a) M. J. Kamlet, R. Taft, *J. Am. Chem. Soc.* **1976**, *98*, 377–383; b) R. Taft, M. J. Kamlet, *J. Am. Chem. Soc.* **1976**, *98*, 2886–2894.

[13] G. Kodali, J. A. Mancini, L. A. Solomon, T. V. Episova, N. Roach, C. J. Hobbs, P. Wagner, O. A. Mass, K. Aravindu, J. E. Barnsley, *Chem. Sci.* **2017**, *8*, 316–324.

[14] a) L. R. Milgrom, M. J. Warren, **1997**; b) R. Giovannetti, in *Macro to nano spectroscopy*, IntechOpen, **2012**.

[15] G. A. Montano, H.-M. Wu, S. Lin, D. C. Brune, R. E. Blankenship, *Biochemistry* **2003**, *42*, 10246–10251.

[16] Y. Li, N. Scales, R. E. Blankenship, R. D. Willows, M. Chen, *Biochim. Biophys. Acta Rev. Bioenerg.* **2012**, *1817*, 1292–1298.

[17] S. He, S. H. Scheres, *J. Struct. Biol.* **2017**, *198*, 163–176.

[18] a) S. Furumaki, F. Vacha, S. Habuchi, Y. Tsukatani, D. A. Bryant, M. Vacha, *J. Am. Chem. Soc.* **2011**, *133*, 6703–6710; b) I. A. Abdourakhmanov, A. O. Ganago, Y. E. Erokhin, A. A. Solov'ev, V. A. Chugunov, *Biochim. Biophys. Acta Rev. Bioenerg.* **1979**, *546*, 183–186; c) H. Van Amerongen, H. Vasmel, R. Van Grondelle, *Biophys. J.* **1988**, *54*, 65–76.

[19] a) V. Agranovich, M. Galanin, *North-Holland* **1982**, 81–170; b) J. M. Linnanto, J. E. Korppi-Tommola, *J. Phys. Chem. B* **2013**, *117*, 11144–11161; c) T. A. Farid, G. Kodali, L. A. Solomon, B. R. Lichtenstein, M. M. Sheehan, B. A. Fry, C. Bialas, N. M. Ennist, J. A. Siedlecki, Z. Zhao, *Nat. Chem. Biol.* **2013**, *9*, 826.

[20] a) G. Pescitelli, S. Gabriel, Y. Wang, J. Fleischhauer, R. W. Woody, N. Berova, *J. Am. Chem. Soc.* **2003**, *125*, 7613–7628; b) N. Harada, K. Nakanishi, *Acc. Chem. Res.* **1972**, *5*, 257–263; c) J. A. Schellman, *Acc. Chem. Res.* **1968**, *1*, 144–151.

[21] D. S. Tyson, C. R. Luman, F. N. Castellano, *Inorg. Chem.* **2002**, *41*, 3578–3586.

[22] a) E. Steckhan, T. Kuwana, *Ber. Bunsenges. Phys. Chem.* **1974**, *78*, 253–259; b) C. Bird, A. Kuhn, *Chem. Soc. Rev.* **1981**, *10*, 49–82.

[23] a) E. M. Kosower, J. L. Cotter, *J. Am. Chem. Soc.* **1964**, *86*, 5524–5527; b) D. R. Senn, P. W. Carr, L. N. Klatt, *Anal. Biochem.* **1976**, *75*, 464–471; c) T. M. Bockman, J. K. Kochi, *J. Org. Chem.* **1990**, *55*, 4127–4135; d) S. G. Mayhew, *Eur. J. Biochem.* **1978**, *85*, 535–547.

Manuscript received: March 1, 2019
Revised manuscript received: March 9, 2019
Version of record online: May 2, 2019